International Journal of Nanomedicine

Dovepress
open access to scientific and medical research

Open Access Full Text Article

ORIGINAL RESEARCH

Doxorubicin/Cisplatin-Loaded Superparamagnetic Nanoparticles As A Stimuli-Responsive Co-Delivery System For Chemo-Photothermal Therapy

This article was published in the following Dove Press journal:
International Journal of Nanomedicine

Mona Khafaji[1]
Masoud Zamani[2]
Manouchehr Vossoughi[2,3]
Azam Iraji zad[1,4]

[1]Institute for Nanoscience and Nanotechnology, Sharif University of Technology, Tehran 14588-89694, Iran; [2]Institute for Biotechnology and Environment (IBE), Sharif University of Technology, Tehran, Iran; [3]Department of Chemical and Petroleum Engineering, Sharif University of Technology, Tehran, Iran; [4]Department of Physics, Sharif University of Technology, Tehran 14588, Iran

Introduction: To date, numerous iron-based nanostructures have been designed for cancer therapy applications. Although some of them were promising for clinical applications, few efforts have been made to maximize the therapeutic index of these carriers. Herein, PEGylated silica-coated iron oxide nanoparticles (PS-IONs) were introduced as multipurpose stimuli-responsive co-delivery nanocarriers for a combination of dual-drug chemotherapy and photothermal therapy.

Methods: Superparamagnetic iron oxide nanoparticles were synthesized via the sonochemical method and coated by a thin layer of silica. The nanostructures were then further modified with a layer of di-carboxylate polyethylene glycol (6 kDa) and carboxylate-methoxy polyethylene glycol (6 kDa) to improve their stability, biocompatibility, and drug loading capability. Doxorubicin (DOX) and cisplatin (CDDP) were loaded on the PS-IONs through the interactions between the drug molecules and polyethylene glycol.

Results: The PS-IONs demonstrated excellent cellular uptake, cytocompatibility, and hemocompatibility at the practical dosage. Furthermore, in addition to being an appropriate MRI agent, PS-IONs demonstrated superb photothermal property in 0.5 W/cm^2 of 808 nm laser irradiation. The release of both drugs was effectively triggered by pH and NIR irradiation. As a result of the intracellular combination chemotherapy and 10 min of safe power laser irradiation, the highest cytotoxicity for iron-based nanocarriers (97.3±0.8%) was achieved.

Conclusion: The results of this study indicate the great potential of PS-IONs as a multifunctional targeted co-delivery system for cancer theranostic application and the advantage of employing proper combination therapy for cancer eradication.

Keywords: iron oxide nanoparticles, chemo/photothermal therapy, dual-drug delivery, control release

Correspondence: Mona Khafaji
Institute for Nanoscience and Nanotechnology, Sharif University of Technology, PO Box 11365-11155, Tehran 14588-89694, Iran
Tel +98-21-66164123
Fax +98-21-66164117
Email mona.khafaji@gmail.com

Manouchehr Vossoughi
Department of Chemical and Petroleum Engineering, Sharif University of Technology, PO Box 11365-8639, Tehran, Iran
Tel +98-21-66164104
Fax +98-21-66005417
Email vosoughi@sharif.edu

Introduction

Cancer is the second leading global cause of death that inflicts more people every year as lifestyles change and breast cancer is the most prevalent cancer type among females, with one in every eight women suffering from it in their lifetime.[1,2] The current clinical cancer therapies including chemotherapy, radiotherapy, and surgery lack the desirable effectiveness and are associated with severe side effects.[3–5] For these reasons, finding an improved cancer therapy method has been the subject of extensive research efforts worldwide.

It has been proven that a mixed use of anticancer drugs and/or treatment methods enhances the treatment efficiency by synergistic therapeutic effect and by overcoming

drug resistance.[6,7] Today, clinics practically benefit from the enhanced therapeutic effect of radiotherapy and/or dual drug chemotherapy by two drugs of different action mechanisms after the surgery has been performed. Nevertheless, due to the nonspecificity and high dosage of drugs in these methods, a combined use of them intensifies the side effects and deteriorates the quality of life for patients.[8,9] Over the last decade, with advancement in science and technology, scientists have sought a combination therapy for enhancing the therapeutic index while reducing side effects. In this regard nanotechnology has been the most sought after science to which the major share of research in this field is dedicated. The unique properties that some materials represent at the nanoscale enable them to be used for innovative applications; due to their very small size and surface properties, some types of nanoparticles can accumulate in specific tissues or cells and demonstrate a great potential for application in cancer diagnosis and therapy.[4,6,10] The application of nanostructures as drug carriers[11] and bioimaging[12] and thermal treatment agents[13] has been studied for more than a decade. Some of these nanostructures, eg gold[13-15] and iron,[16] can produce heat as a response to external stimuli such as a magnetic field or laser irradiation. By specific surface modification of these nanoparticles, anticancer drugs can be loaded on them making them good candidates for a combination chemo and thermal therapy.[12,17] However, sometimes the high degree of complexity of the synthesis and modification process practically limits the applicability of nanostructures.

Among all the investigated nanostructures superparamagnetic iron oxide nanoparticles (SPIONs) have attracted extensive attention in cancer therapy due to their significant biocompatibility, biodegradability, ease of synthesis and surface modification, magnetic targeting[18] excellent contrast for magnetic resonance imaging (MRI)[19] and application in thermal treatments.[19,20] SPION-based nanostructures with various modifications have been studied as simultaneous drug carriers and hyperthermia agents.[21,22] However, since their application as photothermal agents in comparison to magnetic hyperthermia provides a better control over the temperature increase – it increases the temperature in the exact target site – most modifications on SPIONs in the recent years have been performed with the goal of combination chemo- and photothermal-therapy.[17,23–25]

The primary goal of all the research efforts in this area is to achieve a more effective therapy with minimized side effects. Diverse novel nanostructures have been studied but they could not always improve the therapeutic index. Indeed, although these new structures have their own merits, the employed design failed to improve the efficacy of both drug delivery and photothermal therapy. Therefore, the maximum cytotoxicity was achieved when the amount of drug was rather significant or an unsafe laser power was applied.[26–28] For example, incorporation of graphene into SPION-based nanostructure significantly enhances the drug loading content, yet a desirable photothermal cell killing cannot be achieved unless an intense and unsafe laser power is employed.[29,30] Not to mention, the biocompatibility of graphene is still a challenge for the scientific community as there are numerous contradictory reports on it.[31,32] In order to take advantage of the surface plasmon resonance properties of gold in the photothermal therapy, gold nanoshell was incorporated to SPION-based nanocarriers. However, due to the weak NIR absorption of spherical gold nanostructures, it was inevitable that a high-intensity laser power would be used to achieve a suitable photothermal cell killing.[14,15] Furthermore, preparation of these nanostructures usually follows a complicated and multi-step synthesis procedure which practically limits their application. Therefore, the need for a safe method with an easily synthesizable structure that could enhance the efficiency of combined chemo-photothermal therapy is well felt.

Herein, for the first time, we present PEGylated silica-coated SPIONs (PS-IONs) as dual drug carriers for Doxorubicin (DOX) and Cisplatin (CDDP), and as photothermal and MRI-contrast agents. By loading two drugs with different action mechanisms on PS-IONs, it would be possible to invade the cancer cells by a three-branched shotgun design, ie targeted drug delivery, dual drug chemotherapy, and photothermal therapy. The physicochemical properties of the synthesized nanoparticles were examined by transmission electron microscopy (TEM), vibrating sample magnetometer (VSM), X-ray diffraction (XRD), Fourier transform infrared spectroscopy (FT-IR), dynamic light scattering (DLS), magnetic resonance imaging (MRI), and by exposure to a 808 nm laser beam. The cytocompatibility and cellular uptake of PS-IONs were investigated both quantitatively and qualitatively using fibroblast and breast cancer cells, respectively. The influence of PS-IONs on blood coagulation cascade and red blood cells was also studied. Furthermore, the performance of PS-IONs as a controlled release system was measured by in vitro simulating the photothermal therapy and acidic cancerous condition. Finally, the effectiveness

of combined therapy on the viability of breast cancer cells was investigated.

Materials And Methods

Materials

Iron (III) chloride hexahydrate ($FeCl_3.6H_2O$), iron (II) chloride tetrahydrate ($FeCl_2.4H_2O$), chromium trioxide (CrO_3), polyethylene glycol (PEG, Mw 6 kDa), methoxypolyethylene glycol (m-PEG, Mw 6 kDa), ammonia (NH_3, 25%), tetraethylorthosilicate (TEOS), potassium chloride (KCl), disodium hydrogen phosphate (Na_2HPO_4), potassium dihydrogen phosphate (KH_2PO_4), sodium chloride (NaCl), ethylenediaminetetraacetic acid (EDTA), acetone, and isopropanol were purchased from Merck. Cis-diammineplatinum (II) dichloride (CDDP), (3-aminopropyl) trimethoxysilane (APTMS), N-(3-dimethylaminopropyl)-Hydroxysuccinimide (NHS), trypsin, penicillin-streptomycin, and 3-(4, 5-dimethylthiazol-2-yl)-2, 5-diphenyltetrazolium bromide (MTT) were obtained from Sigma-Aldrich.

The dicarboxylate-PEG and carboxylated m-PEG were achieved from oxidation of PEG and m-PEG using Jone's reagent as described by Lele.[13,33]

Hydrochloric acid (HCl, 37%) and methanol were purchased from Chemlab (Belgium). Doxorubicin hydrochloride (DOX) was obtained from Pfizer (Perth, Australia). Fetal bovine serum (FBS), RPMI 1640 and high glucose DMEM cell culture mediums were purchased from Thermo Fisher Scientific (Gibco, USA).

All chemicals were of analytical grade and used as received without further purifications. Deionized (DI) water with a resistivity of 18.2 MΩ and double distilled water were used for the preparation of all chemical and biological samples, respectively.

Synthesis Of PS-IONs

The sonochemical method was used to synthesize iron oxide nanoparticles (IONs) in order to achieve smaller particles with a narrow size distribution.[34] Briefly, $FeCl_2.4H_2O$ (0.002 moles) and $FeCl_3.6H_2O$ (0.004 moles) were dissolved in 2 M HCl and titrated with 4% ammonia solution at 30–32°C in the ultrasonic bath for 1 hr. The produced particles were immediately rinsed several times with methanol to neutralize the pH and were dispersed in 50 mL of absolute ethanol.

In the next step, IONs were coated by silica according to Stöber's method.[34] 30 mL of the just-prepared IONs suspension was alkalinized to pH 8–10 using diluted ammonia solution and was put in an ultrasonic bath at 30–32°C. After 15 min, 1.8 mL of TEOS was added to the suspension. After 1 hr, 25 µL of APTMS was added to the reaction mixture to cease the silica coating process and also to functionalize the surface with amine groups.

Finally, the as-prepared core-shell nanostructures were separated from the solution by the use of an external magnetic field and rinsed three times with ultrapure water and was diluted to 30 mL. The structures were then further modified with a layer of dicarboxylate PEG (6 kDa) and carboxylated-methoxypolyethylene glycol (6 kDa) to improve their biocompatibility and drug loading capability. To this end, 1 mL of the silica-coated SPIONs suspension was diluted 5 times and was sonicated for 5 min. Then a diluted solution of an extra amount of dicarboxylate PEG (18 mg) and m-PEG (36 mg) was added to the silica-coated iron oxide nanoparticles and stirred with an equivalent amount of EDC (1.7 mg)/NHS (1 mg) for 2 hrs. The final product was rinsed three times and kept as a suspension in ethanol for future use.

Characterization Of The PS-IONs

Furier transform infrared spectra were recorded on an ABB Bomem MB-100 spectrometer in the range of 400–4000 cm^{-1}. Magnetic properties of Fe_3O_4 nanoparticles (IONs) and PS-IONs were evaluated by MDK Kawir Magnetic vibrating sample magnetometery. The applied magnetic field was in the range of 0 to 9 kOe. The morphology of PS-IONs was observed by transmission electron microscopy (Zeiss EM10C, 80 kV). Crystallographic information and mean particle size of samples were obtained from X-ray diffraction. A P Analytical X'Pert PRO MPD (The Netherlands) X-ray diffractometer with CuKα-irradiation (λ= 1.5406 °A, $10^o < 2\theta < 80^o$) was used to measure the X-ray diffraction patterns.

The platinum concentration was quantified using inductively coupled plasma optical emission spectroscopy (ICP-OES, SPECTRO ARCOS). The fluorescence spectra of doxorubicin were collected on a fluorescence spectrophotometer (Varian, Cary Eclipse) at room temperature.

Magnetic resonance images were recorded using a 3 T clinical MRI scanner (Magnetotrio, Siemens). The relaxivity was determined using spin-echo acquisition utilizing a repetition time (TR) of 3000 ms and 32 echo-times (TE) ranging from 12 to 384 ms where the field of view was 7 cm, slice thickness was 3 mm and acquisition matrix was 256×128. The transverse relaxation time (T_2) of water protons was obtained by fitting a logarithmic curve to the mean of the measured MR signals. By linear least square

fitting of $1/T_2$ (s^{-1}) versus iron concentration (mM) the transverse relaxivity, $r_{2,}$ was calculated.

All the samples were irradiated by a Hi-Tech Optoelectronic (China) optic fiber coupled continuous wave diode laser at 808±5 nm (0.5 W/cm^2).

In Vitro Cellular Assay

Cell Culture

Human breast cancer cells (MCF7; National Cell Bank of Iran) and a mouse fibroblast cell line (L929; National Cell Bank of Iran) were used as a model of cancer and normal cells to evaluate the cytotoxicity of PS-IONs. The MCF7 and L929 cells were cultured in high glucose DMEM and RPMI mediums contained 10% FBS and 1% penicillin/streptomycin, respectively. The cultures were incubated at 37°C in a humidified atmosphere of 5% CO_2.The mediums were replaced every other day and upon 70% confluency, the cultures were subcultured.

Cell Viability Assay

MTT assay was carried out to determine the viability of normal fibroblast cells after one, two, and three days of cell culture in the presence of different amounts of PS-IONs. Briefly, 1 mL of cell suspension (50,000 cells/mL) were plated in plasma treated 24-well plates and cultured for 24 hrs to allow them to attach, and then exposed to a serial concentration of PS-IONs in nine different groups (10 to 500 µg/mL) and further incubated at 37°C in a humidified atmosphere of 5% CO_2. The cell viability was measured using MTT assay standard protocol.[13] The percent of cell viability was calculated as follows:

$$\%\,\text{cell viability} = \frac{\text{absorbance of samples} - \text{absorbance of blank}}{\text{absorbance of control} - \text{absorbance of blank}} \times 100 \quad (1)$$

MTT assay was also performed in order to compare the cytotoxicity effect of CDDP and DOX with that of PS-IONs and drug-loaded PS-IONs on MCF7 human breast cancer cells. The laser effect was also evaluated on each group and results were presented as the average records of three replications. Briefly, the one-day cultured cells (33 wells, 50,000 cells/well) were divided into eleven groups and exposed to a defined concentration of the drugs and/or PS-IONs, as presented in Table 1. After overnight incubation, in order to study the photothermal therapy effectiveness of PS-IONs, samples of five groups were exposed to a laser beam (0.5 W/cm^2, 10 min) and further incubated overnight. The viability of the cells in each group was measured using MTT standard protocol at the end of the third day.

Cellular Uptake

An elemental analysis method was used to quantitatively examine the cellular uptake of PS-IONs. To do so, MCF7 cells (50,000 cell/well) were seeded in 24-well plates and cultured overnight. Then, the culture medium was replaced with a new medium containing a series of PS-IONs concentrations followed by incubation at 37°C for 24 hrs. After rinsing with phosphate buffer saline (PBS) solution (1 mL×3), the cells were detached using trypsin solution and collected in separate vials. The cells were then disintegrated using a high concentration nitric acid at 70°C to release the PS-IONs in the solution for elemental measurement by ICP-OES. Non-treated cells were used as blank and results were averaged from three replications.

In Vitro Hemocompatibility Assay

APTT and PT assay: Prothrombin time (PT) and activated partial thromboplastin time (APTT) were applied to evaluate the thrombogenic activities of PS-IONs. Briefly, a specific amount of 2 mg/mL PS-IONs suspension in PBS was mixed with the human blood plasma which was drawn from healthy adult volunteer and mixed with 3.2% sodium citrate as an anticoagulation agent to obtain the final concentration of 200 µg/mL of PS-IONs and incubated for 30 min at 37°C. Afterward, to 0.1 mL plasma solution, the specific reagents of PT and APTT test were added and left in 37°C for 3 min. Finally, using a photo-optical clot detection instrument (Coatron M1, TECO, Germany), the clotting times were recorded.

Peripheral blood smear test: To obtain a suspension of 200 µg/mL of PS-IONs, a specific amount of 2 mg/mL PS-IONs suspension in PBS was mixed with fresh blood (EDTA-anticoagulated) and was shacked continuously for 10 mins. Then in 40 min time intervals a drop of the blood sample was spread on a glass coverslip followed by fixation with methanol at room temperature then the blood cells were dyed using Giemsa stain.

It should be mentioned that the use of relevant human material was approved by Pasteur Institute of Iran ethics committee. For all the investigations involving human subjects (cellular and blood experiments), a written informed consent has been obtained from the involved participants.

Table 1 Characteristics Of Eleven Groups For Cytotoxicity Assessment By MCF-7 Breast Cancer Cells

Group No.	Control	DOX (4.2 μg/mL)	CDDP (2.8 μg/mL)	PS-IONs (200 μg/mL)	Drug-Loaded PS-IONs	Laser
1	✓					
2	✓					✓
3		✓				
4		✓				✓
5			✓			
6			✓			✓
7		✓	✓			
8				✓		
9				✓		✓
10					✓	
11					✓	✓

Drug Loading And Release

In order to load the drugs on the nanoparticles, 30 mg of PS-IONs was dispersed in 30 mL of deionized water. Different amounts of DOX and CDDP were added to the suspension to reach the final concentration of 15–40 ppm for each of them and the mixture was shaken for 72 h at room temperature. Then, the drug-loaded nanoparticles were separated using an external magnetic field and rinsed several times with deionized water to remove the unattached drugs. All supernatants containing the unloaded DOX and/or CDDP were collected. The amount of unloaded DOX was determined by measuring fluorescence emission at 592 nm (excitation at 485 nm). The amount of unloaded CDDP was calculated by measuring the platinum content using an elemental analysis (ICP–OES) relative to a calibration curve obtained under identical conditions. The drug loading content (DLC) and drug loading efficiency (DLE) were calculated according to equations 2 and 3, respectively.

$$DLC = (W_D/W_n) \times 100 \quad (2)$$

$$DLE = \left(\frac{W_t - W_u}{W_t}\right) \times 100 \quad (3)$$

where the W_D, W_n, W_u, and W_t are weights of the loaded drug, nanoparticles, unloaded drug, and initially added drug, respectively.

To study the release profile of DOX and CDDP from the nanocarriers, a dialysis process was performed. All release studies were performed under sink conditions (amount of drug <10% of the solubility). To this end, 1 mg of drug-loaded nanoparticles were dispersed in 5 mL of PBS and dialyzed against 30 mL of PBS using a 10 kDa dialysis bag (Sigma) in two different pH values of 7.4 and 5.5 at 37°C under constant shaking at 150 rpm. In order to simulate the photothermal condition, a separate group of each pH value was subjected to a 30 min temperature increase to 42°C. At predetermined time intervals, 5 mL of the solution outside the dialysis bag was withdrawn for analysis and replaced with the same volume of fresh PBS solution.

Statistical Analysis

Statistical package for social science (SPSS v. 25.0) software was used for statistical analysis of all the experiments. Multiple samples were analyzed by one-way ANOVA. To compare the control samples with the treated ones, the Student–Newman–Keuls post hoc test was done. Measures are reported as means ± standard deviations and statistically significant difference was reported at $p < 0.05$. The XRD data were analyzed using X'Pert HighScore Pluse software. All the graphs were plotted by Microsoft Excel 2010 software.

Results And Discussion

Synthesis Of PS-IONs

Iron oxide nanoparticles (IONs) were first synthesized through the sonochemical method and then coated with a silica shell to improve their biocompatibility, thermal stability, and dispersibility in aqueous solutions.[34] This relatively simple method also enables the functionalization of the particles' surface for further applications. APTMS was used to both halt the increase-in-thickness of the silica shell on the IONs and to functionalize the surface of silica coated-IONs with amine groups. The zeta potential of the NH_2 modified silica-coated IONs was 27.7 mV. The presence of amine groups on the surface not only enhances the stability of particles due to their positive charge but

also enables the attachment of PEG molecules from their carboxylic acid ends.

After preparation of the silica-coated IONs, their surfaces were modified with PEG to increase their circulation time in the bloodstream and enhance their drug loading ability for targeted drug delivery application. After pegylation, the zeta potential of nanoparticles decreased to −2.27 mV which confirms the presence of the COOH groups on the surface of PS-IONs instead of NH_2 ones. The detailed procedure for the preparation of the PS-IONs and the drug loading on them is illustrated in Scheme 1.

Figure 1a and b show the TEM images of the PS-IONs. It could be observed that the nanoparticles were spherical in shape with a narrow size distribution and an average size of 20±3 nm. The IONs could be distinguished from the silica through the difference in their contrasts.

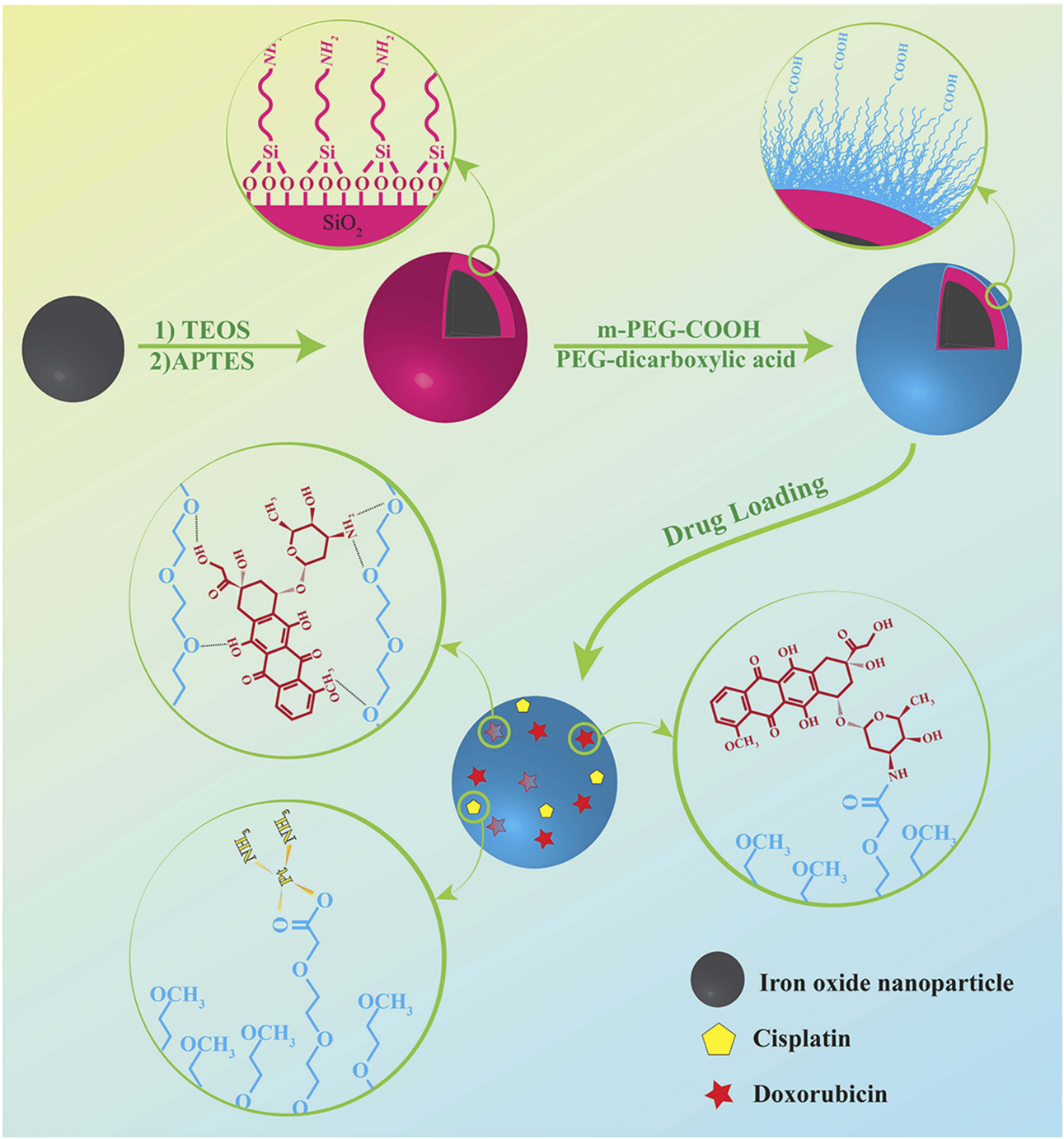

Scheme 1 Illustration of the synthesis procedure of PS-IONs and drug loading mechanism.

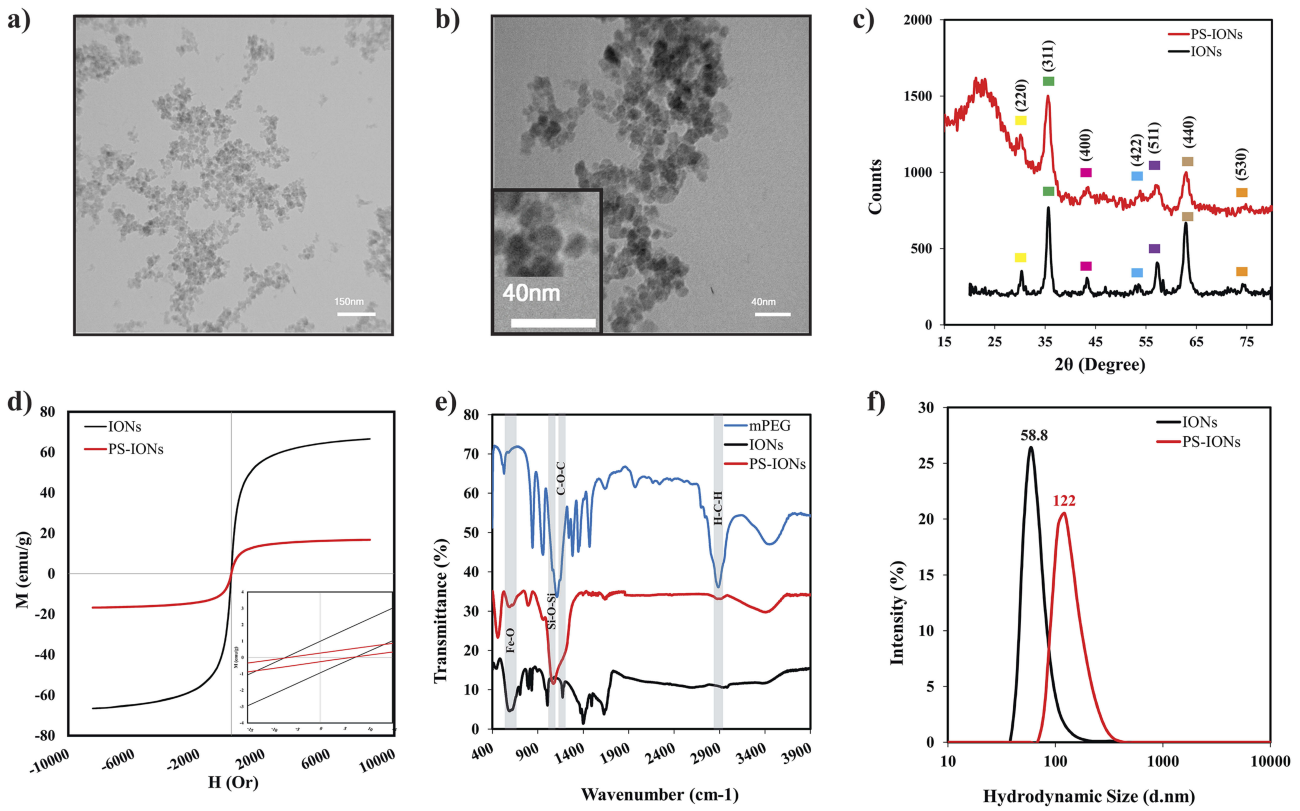

Figure 1 (**a, b**) TEM images of PS-IONs (scale bars are 150 nm and 40 nm, respectively). (**c**) XRD patterns [the yellow, green, pink, blue, violet, light brown and orange squares relate to (220), (311), (400), (422), (511), (440) and (530) planes of the spinel structure of magnetite, respectively], (**d**) hysteresis loops, (**e**) FT-IR spectra, and (**f**) DLS particles size distribution profiles of IONs (black line) and PS-IONs (red line).

According to TEM images, the silica shell was thin enough to limit the adverse effect on magnetization saturation. The severe aggregations of the PS-IONs were presumably due to the hydrogen bonding of PEG molecules among the nanoparticles.

X-ray diffraction (XRD) experiments were also performed to investigate the crystalline structure of IONs and PS-IONs (Figure 1c). The characteristic diffraction peaks in both spectra could be assigned to the (220), (311), (400), (422), (511) and (440) planes of the spinel structure of magnetite (Fe_3O_4) according to the JCPDS 19–0629. Furthermore, the broad peak at around $2\theta = 20°$ indicates the presence of amorphous silica in the synthesized nanoparticles.[35] The Scherer equation was employed to calculate the average crystallite size from the (311) peak in each spectrum. The calculated particle size for both samples was 15 nm which is in agreement with the observations of the TEM images indicating that the silica coating process does not induce major unfavorable effects such as dissolution or growth of the crystals on the Fe_3O_4 nanocrystals.

Considering that the size of PS-IONs was less than a magnetic domain for these components (25 nm for Fe_3O_4), it was expected that they possess a superparamagnetic behavior.[34] With this in mind, VSM analysis was performed on PS-IONs to evaluate their magnetic behavior (Figure 1d). The results show that the magnetization saturations of the IONs and PS-IONs were 66.6 $emug^{-1}$ and 16.75 $emug^{-1}$, respectively. These data were consistent with the previous observations which indicate that silica coating decreases the magnetization saturation of IONs by at least four folds.[36] The magnetic residue of both IONs and silica-coated ones were 4mT, hence both samples were classified as superparamagnetic nanoparticles.[34] The superparamagnetic behavior in silica-coated particles possibly results from bipolar-bipolar interactions between the magnetic cores. Therefore, since the bipolar-bipolar magnetic interactions had a reverse relationship with the distance, the interactions were intensified as a result of the entrapment of more than one ION in a silica shell and/or the physical attachment by the hydrogen bonding of PEG molecules.[19,34]

FT-IR spectroscopy was employed to verify the formation of the silica shell surrounding the Fe_3O_4 nanoparticles and also to investigate the success of the PEGylation process. Figure 1e shows the IR spectra of IONs (black),

PS-IONs (red), and PEG (blue). The presence of silica, magnetite, and PEG in the PS-IONs was clearly shown by the observation of the characteristic bands of all three, magnetite (560, 1400 cm^{-1}, Fe-O band vibration), silica (1080 cm^{-1} asymmetric Si-O-Si stretching), and PEG (2925 cm^{-1} CH_2 stretching vibration, 1150 cm^{-1} C-O-C stretching), in the PS-IONs' spectrum (red line). There was also an evidence of bonds formation between silica and Fe_3O_4 (1190 cm^{-1}, Fe-O-Si vibration) confirming the formation of the desired structure. Unlike the IONs, dissolving the PS-IONs even in hot hydrochloride acid (37% w/v) was not possible except after prewashing in a hydrofluoric acid to remove the silica coating, endorsing the full coverage of silica on the nanoparticles.

The hydrodynamic size of the nanoparticles in aqueous solution was determined by DLS (Figure 1f). The results showed a single peak with a small polydispersity index which points to the negligible aggregation of PS-IONs in aqueous solution. The average diameters in a hydrated state were 58.8 (PDI=0.171) and 122 nm (PDI=0.156) for IONs and PS-IONs, respectively. The measured size of IONs by the DLS method was significantly higher compared to the TEM measurements. According to previous reports, this may be occurred due to the fast flocculation of bare magnetic nanoparticles, the presence of water molecules on their surface, and/or the magnetic dipole-dipole attraction between magnetic nanoparticles.[37–39] Also, the measured size for PS-IONs was approximately six times higher than that measured by TEM. This increase may be due to the fact that more than one ION was trapped in the same silica coat and/or irreversible aggregates formed through the PEG bridges. In addition the hydrophilic PEG chains were extended in the aqueous solution or/and dynamic association in the liquid.[8,34] In view of the fact that the nanocarriers' size plays an important role in their biodistribution and accumulation in the organs and cells, the synthesized PS-IONs are absolutely ideal as nanocarriers for cancer therapy applications.

In Vitro Cytocompatibility

The most important characteristic of a nanocarrier in a given drug delivery application is its negligible toxicity to normal cells. The cytotoxic effects of PS-IONs on L929 fibroblast cells were evaluated by conducting a MTT assay. Figure 2 shows that the presence of nanoparticles did not induce any significant detrimental effect on the viability of normal cells at 24, 48, and 72 h time points. The viability of cells was more than 88±5.2% even after exposure to 500 µg/mL of nanoparticles for 72 h, endorsing the success of the employed surface

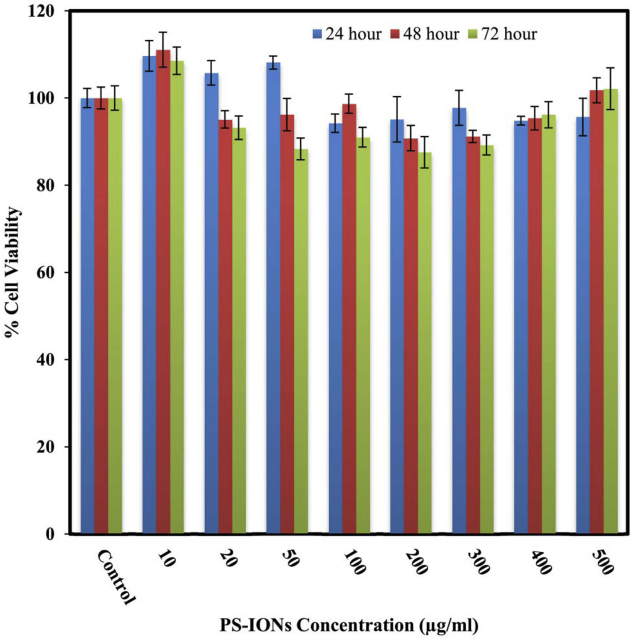

Figure 2 Viability of L929 normal fibroblast cells after 24, 48, and 72 hrs of incubation with different concentrations of PS-IONs (ranging from 10 to 500 µg/mL). There was no significant difference between the control and other groups.

modification in the improvement of the nanoparticles' biocompatibility.[40] Unlike some of the previous observations, the increase in the cell density in comparison to the control in some samples is attributed to their metabolic changes after being exposed to nanoparticles rather than the dissolution of IONs.[19] Light microscopy images of the cells exposed to different concentrations of PS-IONs for defined times indicated that the presence of the nanoparticles in the culture medium had no adverse effect on the attachment and morphology of the cells (Figure S1). This significant improvement in the biocompatibility was attributed to both the silica coating and the PEGylation which makes the prepared particles suitable candidates for a drug delivery application.

Cellular Uptake

It is essential for the nanoparticles to internalize into target cells in the highest amount in order to be considered as effective drug delivery vehicles. The cellular uptake of PS-IONs by MCF7 breast cancer cells was studied both quantitatively and qualitatively. According to Figure 3a, the PS-IONs could be obviously visualized in the cytoplasm of the cells as brown spots indicating that their accumulation in the cells did not affect the cells' normal morphology. In addition, the cumulative cellular uptake of PS-IONs was linearly increased as their concentration in the medium increased up to 200 µg/mL. The percentage of the uptaked PS-IONs increased linearly at low

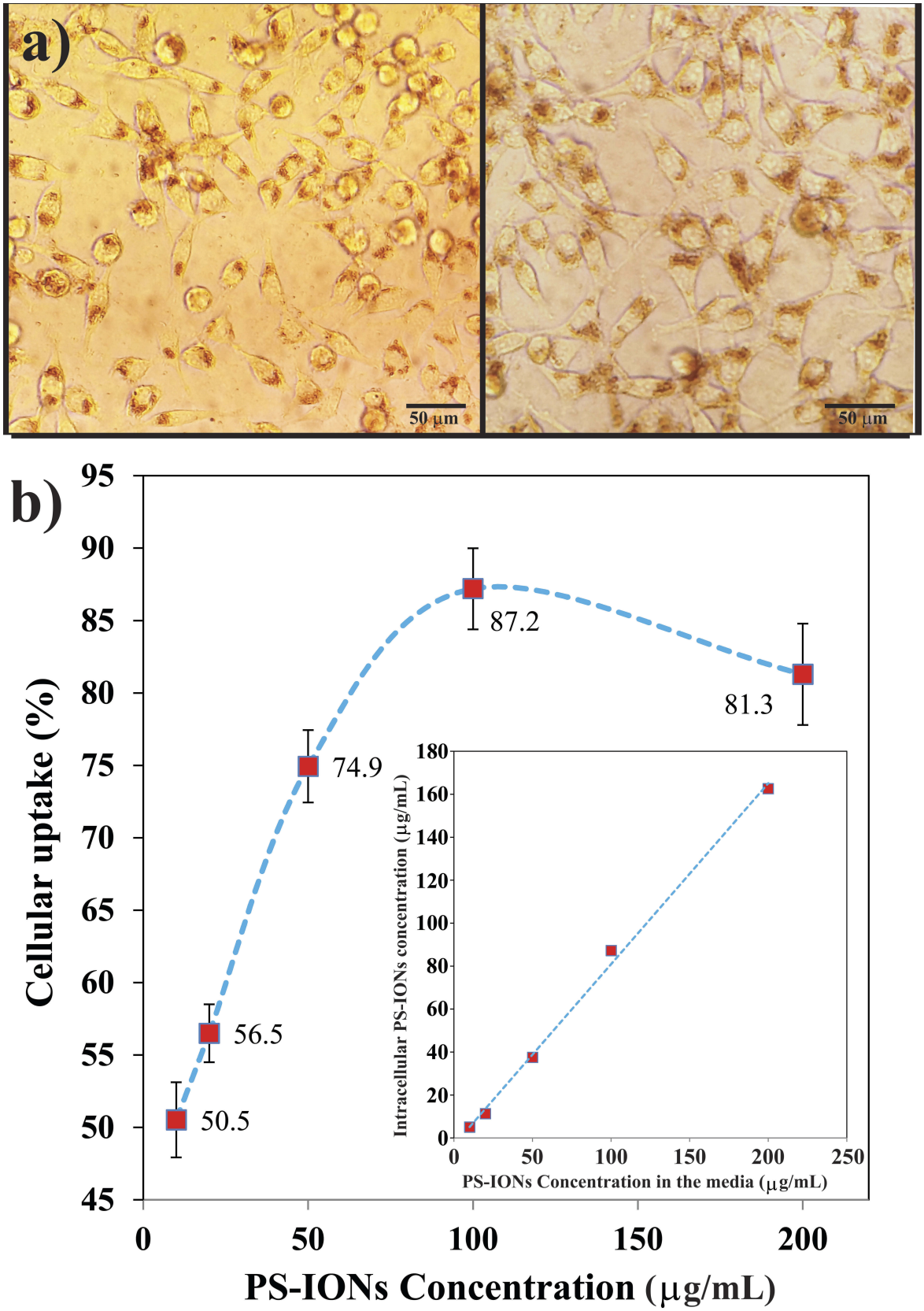

Figure 3 (**a**) Light microscopy images of the cells (the total magnification was 400 times) exposed to 100 (left) and 200 µg/mL (right) of PS-IONs for 24 hrs. The brown dots show the uptaken nanoparticles. (**b**) Concentration dependent cellular uptake percentage. The inset shows the amount of PS-IONs uptake (µg/mL) versus initial PS-IONs concentration (µg/mL) in the culture media.

concentrations (up to 50 μg/mL), while further increase of the PS-IONs concentration in the culture medium caused their uptake rate to decelerate so that for concentrations above 100 μg/mL the uptake percentage declined indicating the cells were approaching their saturated uptake capacity (Figure 3b). This excellent cellular uptake was related not only to the optimum particle size and the spherical morphology of PS-IONs but also to their surface characteristics. By altering the serum protein adsorption on the nanoparticles surface, the coating affects the nanoparticles-cells interactions and thus improved the cellular uptake.[41,42] So, the presence of PEG on the particles surface improved the cellular uptake and viability through prevention of the attachment of proteins to their surface.[43,44]

In Vitro Hemocompatibility

Another determinant factor in the clinical applicability of nanocarriers is their means of interaction with the blood cells. A proper drug delivery system should not induce any adverse effect on the morphology and activity of the blood cells.[45] Accordingly, the hemocompatibility of the as-synthesized nanoparticles was investigated by studying their effect on blood coagulation and the morphology of red blood cells (RBCs).[13,46,47] The coagulation times in the presence of PBS (control) and 200 μg/mL of PS-IONs were investigated. The results showed that the PT and APTT have not been affected in the presence of such a high concentration of nanoparticles and still remained in the normal reference range (Table 2).

Normally RBCs have a biconcave disk shape which easily changes in interaction with foreign substances.[13,46] The investigation of RBCs morphology, when exposed to a foreign material, is a routine method to evaluate the new biomaterial's hemocompatibility. Hence, the peripheral blood smear test was performed to study the influence of the PS-IONs on the shape of RBCs. It can be observed from Figure 4 and Figure S2 that the RBCs had undergone neither deformation nor aggregation after exposure to the 200 μg/mL of PS-IONs even after 4 hrs of incubation when compared to the controls. This excellent hemocompatibility was attributed to the negligible electrostatic interaction between negatively charged RBCs and PEGylated nanoparticles, resulting from the presence of non-reactive methoxy groups on their surface.

Table 2 Blood Coagulation Times After Dilution With The Same Volumes Of PBS And PS-IONs Suspension (final Concentration Of 200 μg/mL)

	Normal Range	Diluted With PBS	Diluted With PS-IONs (200 μg/mL)
APTT (s)	28 to 38	39.0	38.0
PT (s)	11 to 14	13.0	13.2

In Vitro Drug Loading And Release

The ability of nanoparticles to carry and deliver a sufficient amount of anticancer drug to the tumor tissues is of great importance. Among the various anticancer drugs, CDDP and DOX are widely used for solid cancerous tumor treatment, therefore loading each of them on nanocarriers has been extensively investigated.[48-50] As the various anticancer drugs have different action mechanisms, it has been proven that cancerous cells could be killed more effectively by the use of dual-drug chemotherapy.[8,9] Therefore, the potency of the PS-IONs was examined as magnetically targeted dual-drug carriers by loading both DOX and CDDP on them. The loading efficiency of DOX in the presence of a constant amount of CDDP (15 ppm) was investigated. As shown in Figure 5a the DLC was raised by increasing the initial DOX concentration. At the optimum conditions (30 ppm DOX), the obtained DLE was 69.3±1.4% with DLC of 21±0.42 μg DOX/mg PS-IONs. At the normal pH, DOX has a positive charge while the carboxyl groups on the particles surface were negatively charged.[51] Therefore, DOX could be efficiently loaded into PEG chains through electrostatic interactions, as well as the formation of amide and hydrogen bonds.[11,22]

To investigate the loading of CDDP on the nanoparticles, different concentrations of CDDP were added to the solutions containing constant amounts of DOX loaded PS-IONs (1 mg/mL) and DOX (15 ppm) (Figure 5b). The amount of loaded CDDP obtained in the optimum condition (30 ppm CDDP) was 14±0.4 μg CDDP/mg PS-IONs with a DLE of 46.6±1.4%, resulting in a total DLC of 3.5% w/w. In the absence of DOX, the DLC of CDDP was increased by 100% while the DLE remained unchanged. Hence, the DLE of CDDP is not a function of its initial concentration. It can be concluded that the molecules of both drugs compete against each other to seize the available carboxyl groups on the surface of the particles. So, the higher DLC of DOX in comparison to CDDP is attributed to the higher reaction rate of hydrogen or electrostatic bonding of DOX rather than coordination bonding of CDDP with the carboxyl groups of the particles' surface. After the drug loading, the zeta potential of PS-IONs was changed positively to reach +1.25 mV. According to previous reports, attachment of CDDP and DOX slightly

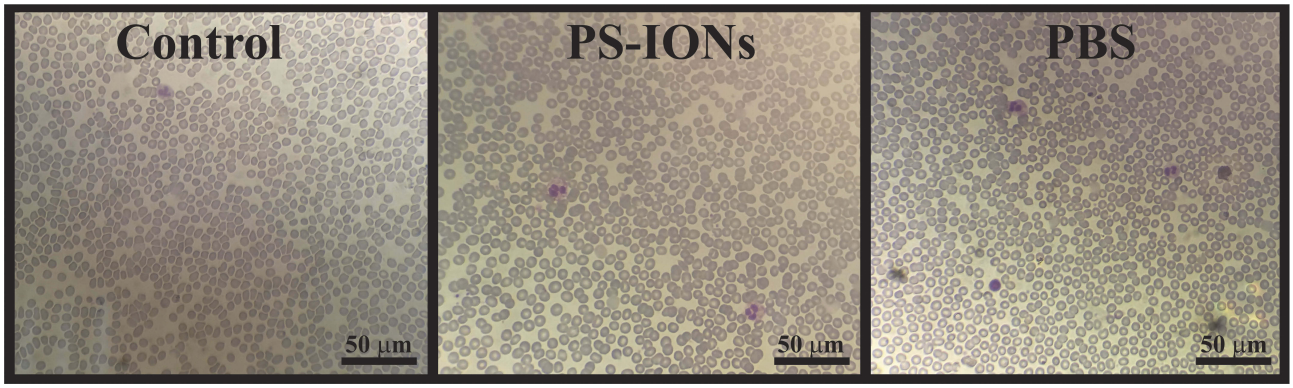

Figure 4 Light microscopy images (the total magnification was 400 times) of blood smear prepared samples from EDTA-anticoagulated blood without dilution (control) and after addition of PS-IONs (final concentration 200 μg/mL) and PBS after 4 h. The RBCs showed neither deformation nor aggregation when compared to the controls.

increase the zeta potential. So the zeta potential changes confirmed the successful drug loading.[52,53] IR spectra of the drug-loaded PS-IONs were also employed to confirm the presence of both drugs on them. As it can be seen in Figure S3, the characteristic peaks of both DOX (3512, 632 cm^{-1}) and CDDP (3296, 1319 cm^{-1}) were presented in the spectrum of the drug-loaded PS-IONs, demonstrating the reliability of the loading method.

Having a controlled drug release in the body and tumor tissues is an indispensable characteristic of a drug delivery system for cancer therapy. Minimizing the drug release in the normal tissues not only reduces the side effects of the drugs, it also maximizes the drug dosage at the tumor site as well, resulting in a more efficient and favorable treatment. To study the in vivo release behavior of drugs from the as-synthesized PS-IONs, the pH conditions of normal and cancerous tissues were simulated in vitro. Furthermore, the effect of photothermal treatment using nanoparticles was investigated by imposing an initial temperature increase to 42°C for 30 min. As shown in Figure 5c only about 23±2.2% of DOX released from the PS-IONs after 24 h at the physiological condition, while the release reached to 41±2.7% and 45±2.6% by decreasing the pH to 5.5 and by applying the photothermal condition, respectively. This indicates that both the temperature increase and the pH decrease stimulate the drug release. Applying the photothermal and acidic pH conditions simultaneously increased the release rate three folds. This pH- and thermo-responsive drug release could be explained according to the drug-PEG interactions. The interaction intensity between DOX molecules (pK_a = 8.2) and PEG chains weakens when decreasing the pH of the media from neutral or weak alkaline to acidic condition. Therefore DOX could remain loaded on the nanoparticles during the blood circulation and could escape from them more easily within the tumor cells. Similarly, through increasing the system's energy level, the temperature rise has the same effect on the interaction intensity between DOX and PEG.[11,22]

As Figure 5D shows, the CDDP release was more temperature-dependent than pH-dependent. As mentioned before, CDDP molecules were loaded through the coordination of interactions between the hydrolyzed drug molecules and the terminated carboxyl groups of PEG. By decreasing the pH, the terminated carboxyl groups were protonated which attenuated the interaction between the drug molecules and the PS-IONs. In addition, according to the equilibrium hydrolysis reaction of CDDP (Figure S4) in acidic conditions and in presence of excess amount of chlorine ions the rate of mono- and dichloro-cisplatin formation increases which results in a faster release of drug molecules. Moreover, through supplying the coordination dissociation energy, higher temperature leads to an increase in CDDP release rate by more than two folds.[54,55] Applying the photothermal treatment and acidic pH conditions simultaneously increased the release rate by 2.7 folds.

The release rate of CDDP in all situations was more than that of DOX (Figure S5) which indicated the difference in drug-PS-IONs interactions. Unlike the CDDP, the DOX molecules could entrap between the PEG chains by hydrogen bonding in addition to the terminal attachment which resulted in the higher DLC.[11,18] This was a reason for the slower release of DOX, because some of the DOX molecules had to diffuse through the PEG chains in order to enter the solution while the terminally-loaded CDDP molecules could directly be released into the solution. These data indicate that the designed dual stimuli-triggered

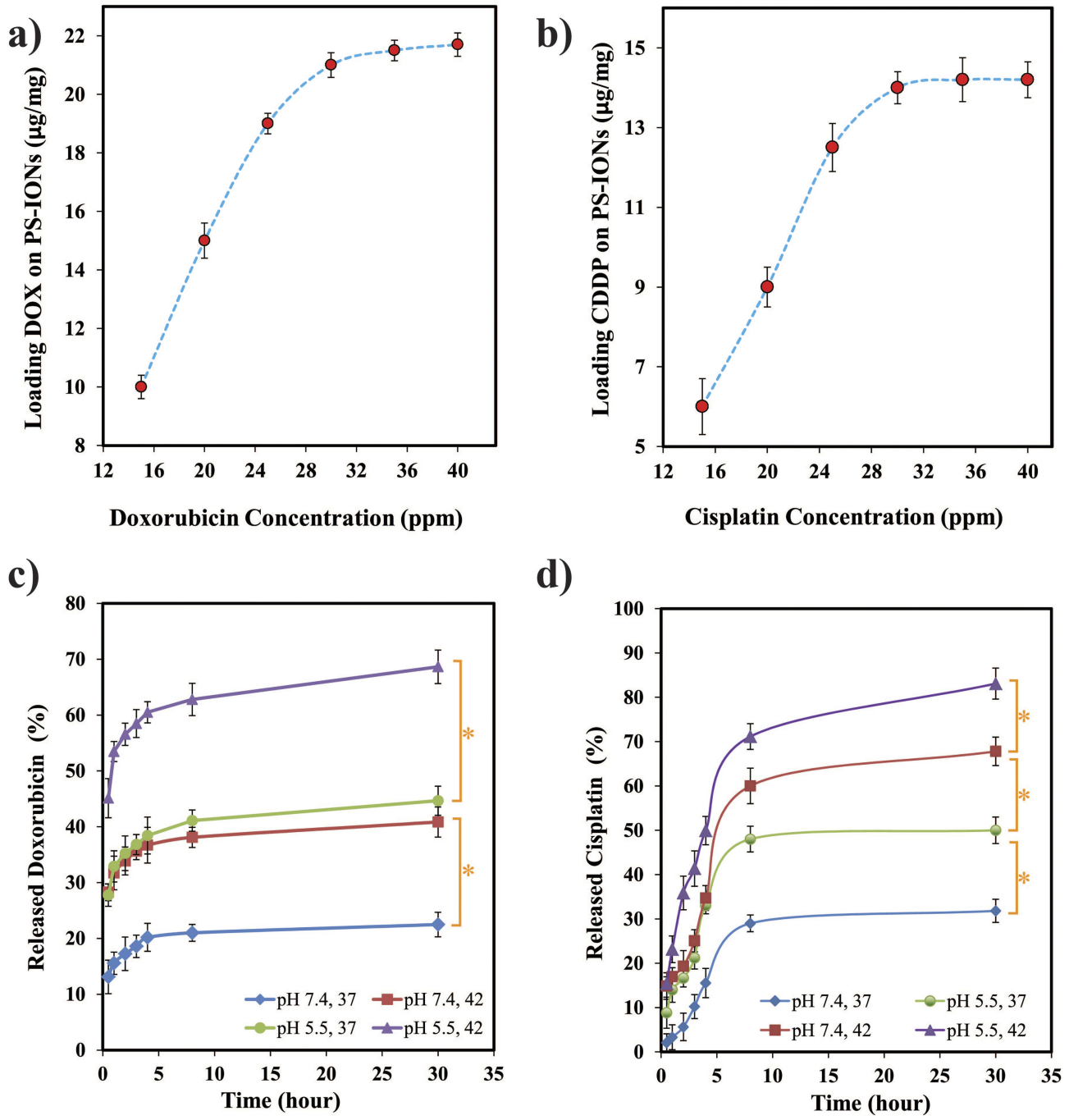

Figure 5 Loading capacity of (**a**) DOX and (**b**) CDDP on PS-IONs as a function of their initial concentation in the solutions containing 15 ppm of CDDP and DOX, respectively. In vitro release profiles of (**c**) DOX and (**d**) CDDP from PS-IONs at different temperature and pH conditions. Asterisks (*) indicate significant difference ($P < 0.05$).

drug release system provides a favorable drug delivery platform for combination with photothermal therapy.

PS-IONs As MRI Contrast Agent

The ability of PS-IONs to serve as MRI contrast agents was investigated using a 3T clinical instrument. The recorded images showed proton relaxation enhancement compared to the deionized water control (Figure 6a). The calculated r_2 for the PS-IONs was 127.31 $mM^{-1}s^{-1}$ (Figure 6b) which is comparable with that obtained for PEGylated or silica coated IONs.[40,56] The obtained transverse relaxivity was almost twice the amount of its bare IONs.[57,58] This enhancement could be explained according to the structural characteristics of PS-IONs. As reported before, the field gradients generated by magnetized nanoparticles resulted in dephasing of the magnetic moment in

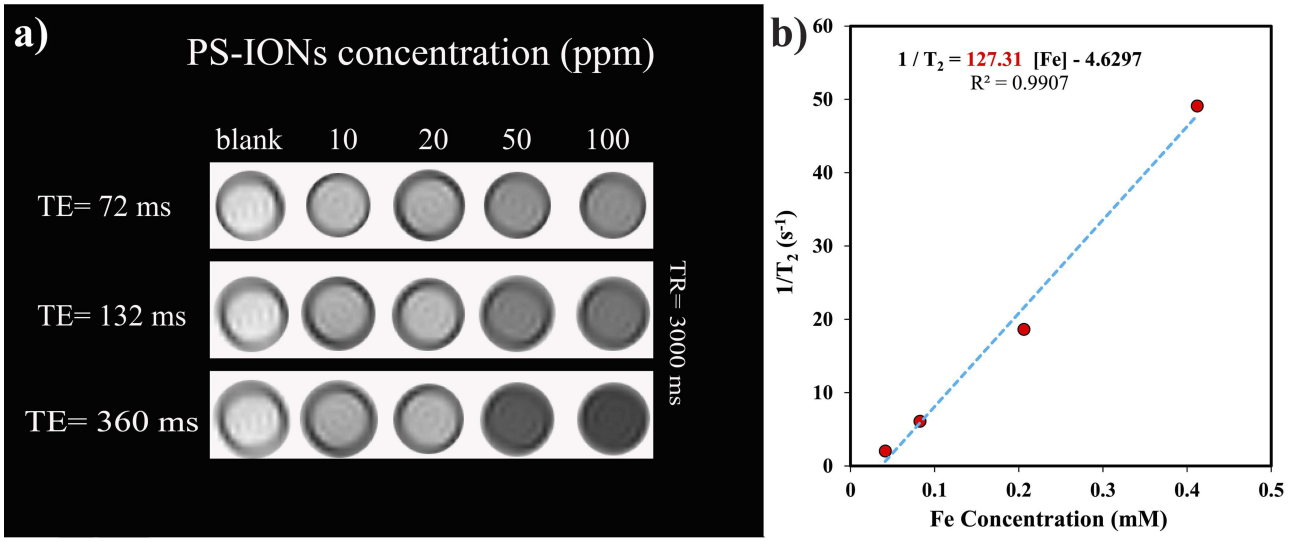

Figure 6 (**a**) T_2-weighted MR images of PS-IONs in aqueous media at various concentrations and different echo times. (**b**) T_2 relaxation rate (R_2) versus iron concentration in PS-IONs.

water's protons. Therefore magnetic nanoparticles induced spin-spin relaxation as the proton passes through such field gradients. By increasing the iron concentration, the magnetic moment becomes stronger resulting in distortion of spin coherence of water protons in transverse relaxation.[56]

The transverse relaxivity is related to the hydrodynamic diameter of the aggregated nanostructure and the magnetic saturation. Although the magnetic saturation of PS-IONs was reduced comparing to its initial value, the significant increase in the PS-IONs hydrodynamic diameter was the leading factor in the MRI contrast enhancement. The PEGylated nanoparticles could make small reversible aggregates through the hydrogen bonding. Formation of these cluster-like structures not only increased the effective hydrodynamic diameter of nanoparticles several times but also shortened the distance among magnetic particles which, in turn, induced a more inhomogeneous local magnetic field. Finally, improved hydrophilicity of PEGylated nanoparticles facilitated the diffusion of water molecules near the surface of magnetic particles, immobilizes them by hydrogen bonding, and extended the interaction between the magnetic field and protons.[56,59]

Cytotoxicity Effect Of Multiple Treatment Method

The efficiency of the multiple-treatment-method was studied on MCF7 breast cancer cells in vitro and was compared with individual chemotherapy and photothermal therapy according to Table 1. The obtained results are summarized in Figure 7. As was expected, the sole laser treatment (0.5 W/cm^2, 808nm) neither had a significant effect on the cells' viability nor exerts an effective interaction with the CDDP and DOX drugs. The viability of the cells exposed to DOX (4.2 µg/mL) and CDDP (2.8 µg/mL) for 48 h, were 20.5±4% and 57±5%, respectively. Although the free drugs have significantly decreased the cell viability, these data indicate the inefficacy of the drugs at such low concentrations. This was the reason for the extensive side effects of traditional cancer chemotherapy, as it requires

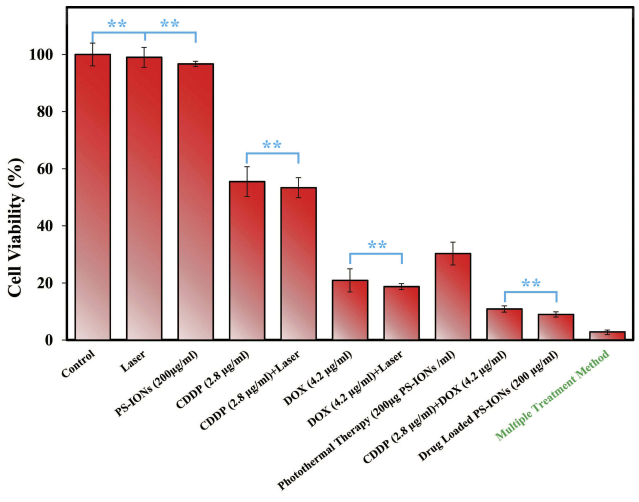

Figure 7 MTT viability assay of MCF7 cells after exposure to 0.5 W/cm^2 near-IR laser irradiation for 10 min, incubation with 200 µg/mL of PS-IONs, chemotherapy with DOX (4.2 µg/mL) or CDDP (2.8 µg/mL), dual-drug chemotherapy, photothermal treatment, and multiple treatment method. Values are mean±SD. Double asterisks (**) indicate nonsignificant difference (P>0.05).

administration of a high dosage of drugs in the whole body to reach a desirable cytotoxicity for tumor cells.[60]

DOX, an anthracycline antibiotic, restrains the DNA remodeling through intercalating between DNA nucleotides and inhibiting the activity of topoisomerase II (TOP2).[61] CDDP, a powerful DNA chelating agent, induces cancer cells apoptosis by covalently bonding with DNA purine bases to form DNA adducts which could inhibit cellular transcription and replication.[62] These two drugs have independent action mechanisms, and consequently, DOX could further impede the repairing of CDDP-damaged DNA by TOP2. Therefore, the combination chemotherapy by DOX and CDDP could disrupt the cellular repair mechanisms. A mixed use of cancer drugs with different mechanisms of action is a clinical method to overcome the cell's resistance. It would also reduce the side effects of treatment by decreasing the administered dosage and improving the treatment efficiency.[8,9,63] As it is shown in Figure 7, dual-drug chemotherapy had significantly enhanced the cytotoxicity so that the cells' viability declined to 10.65±0.9%. This result confirmed the synergetic effect of chemotherapy drugs on the cancer cells.

As it was qualitatively shown in Figure 3, PS-IONs had no unfavorable effect on the cancer cells' morphology. They also demonstrated very good biocompatibility (Figure 2) and excellent cellular uptake. By loading the drugs on these nanocarriers, they would escape the drug resistance by entering the cells through endocytosis enhancing the cytotoxicity.[64,65] The results show that although almost half of each drug were remained loaded on the nanocarriers (50±3% of CDDP and 45±2.6% of DOX, according to in vitro simulation), they resulted in the same cytotoxicity as the free drugs. This was most likely due to the effective cell membrane penetration and accumulation of the drug-loaded PS-IONs into MCF7 cells by endocytosis and phagocytosis. Consequently, this phenomenon increased the accumulated drugs within the cells since they would release more rapidly due to the intracellular acidic condition of cancer cells.[66,67]

In addition to drug delivery, the PS-IONs show remarkable ability as photothermal agents. Free PS-IONs demonstrated superior cytotoxicity over CDDP (2.8 μg/mL) by reducing the cell viability to 30±4%, after an exposure to low power laser irradiation (0.5 W/cm^2, 10 min) which increased the temperature from 37°C to 42°C. In contrast to previous studies, a low power laser irradiation, close to the maximum permissible exposure (MPE) for skin (0.33 W/cm^2), had been used for photothermal therapy.[6,16,24] By emitting the NIR light beam to the drug-loaded PS-IONs, a significant enhancement in cytotoxicity had been obtained. The multiple-treatment-method increased the cancer cell killing efficiency to 97.3±0.8% in a single dose therapy. This result surpasses the best of previously reported outcomes for SPION-based nanocarriers despite the fact that very low drug concentration and laser power intensity is simultaneously employed in our study (Table 3). This excellent result was partly attributed to the higher accumulated free drugs content in the cells as a result of the photothermal and acidic condition in comparison to the non-photothermal condition (see Figure 5). Furthermore, besides the photothermal-induced cytotoxicity, the therapeutic index of CDDP was enhanced by the increase in temperature.[68] Therefore, as a result of cellular internalization, controlled intracellular drug release, dual drug chemotherapy, and photothermal therapy, PS-IONs were an outstanding candidates for cancer therapy applications.

Conclusion

The superparamagnetic PS-IONs were prepared by a relatively simple and efficient sonochemical method. The particles have favorable chemical stability and water dispersibility and also demonstrated excellent bio- and hemocompatibility. The SiO_2 and Fe_3O_4 nanoparticles were known as in vivo biodegradable nanomaterials with non-toxic byproducts.[69] The PS-IONs could act as dual-drug nanocarriers. DOX was loaded on particles by both hydrogen bonding and electrostatic interactions[11,18,22] with DLE and DLC of 63.9% and 2.1%, respectively, while CDDP could efficiently conjugate with carboxyl groups of PEG molecules through coordination interaction resulting in DLE and DLC of 46.6% and 1.4%, respectively. Both drugs had a slow release profile in normal blood conditions. Only 31% of CDDP and 22% of DOX were released during 30 h under normal conditions which significantly decrease the drug accumulation and toxicity in the normal tissues. These drug carriers revealed a dual stimuli-triggered release behavior. High release rates of 69% and 84% were obtained for DOX and CDDP, respectively, during 30 h in a simulated photothermal condition in an acidic cancerous environment. Synergistic photothermal therapy and DOX/CDDP combination chemotherapy could be achieved through the use of PS-IONs nanocarriers. PS-IONs efficiently delivered both DOX and CDDP into the MCF-7 cells and demonstrated potent antitumor activity in vitro which was significantly intensified by exposure to a low power near-IR laser irradiation. As the

Table 3 Summary Of The Parameters And Outcomes Of Some SPION-Based Chemo-Photothermal Therapy Studies

Nanostructure	Concentration (μg/mL)	Laser [(W/cm^2); (λ(nm); t(min)]	Drug; Concentration (μg/mL)	Cell Line	Relaxivity ($mM^{-1}s^{-1}$)	Cyto-toxicity (%)	Comments
This study	200	0.5; 808; 10	DOX; 4.2 CDDP; 2.8	MCF-7	127.31	97.3 ± 0.8	–
rGO-Fe_2O_3@Au NPs[30]	50	2; 808; 5	DOX; 50	HeLa	54.99	~96	–
GO-PEG-γ-Fe_2O_3[29]	Not reported	2; 808; 5	DOX; 6	HeLa	33.15	~93	Loading factor was 1.18
Porous hollow Fe_3O_4[23]	150 μg Fe/mL	1.5; 808; 10	DOX; Not reported	4T1	119.66	~75	–
Lactobionic acid/Fe_3O_4@polydopamine/PEG[73]	125	1; 808; 30	DOX; ~46	HepG2	Not studied	75.4	Cytotoxicity increased to 83.7% after exposure to magnetic field
Fe_3O_4@mSiO_2-PO*-folic acid[26]	125	2; 808; 30	DOX; ~5.6	HeLa	Not studied	81	–
Fe_3O_4@MnO_2@PPy[27]	600	1; 638; 10	DOX; 420	HepG2	Not studied	91.6	Samples were placed in a magnetic field for 30 min
IONPs@AuNPs@SiNWs[15]	300	1; 808; 20	DOX; 50	MCF-7/ ADR	Not studied	90	Samples were placed in a magnetic field for 3 hrs
Cu_9S_5@mSiO_2@Fe_3O_4-PEG[74]	200	0.76; 980; 10	DOX; 25	HeLa	13.583	83	–
Fe_3O_4@MoS_2/PEG/2-deoxy-D-glucose[28]	200	0.5; 808; 3	DOX; ~101	MDA-MB-231	48.86	~70	The cell viability decreased to 1.4% after the second treatment

drug-loaded nanoparticles can enter the cells via endocytosis, they could overcome the P-gp drug resistance mechanism. Moreover, only the free drugs were pumped out by resistance mechanisms of the cells.[64,65,70,71] Also, the Fe_3O_4 nanoparticles may act as the P-gp inhibitor in some drug resistance cancer cells.[72] Therefore, this delivery system can potentially be used for other combination therapies and holds a great promise as an effective tool to treat drug-resistance cancer tumors.

Acknowledgments

The authors gratefully thank Prof. M. Reaz Hormozi-nezhad from the Department of Chemistry of the Sharif University of Technology for his help and support, and Dr. Rabeei and Mr. Shahbazi for doing the blood tests at Vardavard Medical Laboratory.

Author Contributions

All authors contributed to data analysis, drafting and revising the article, gave final approval of the version to be published, and agree to be accountable for all aspects of the work.

Disclosure

The authors report no conflicts of interest in this work.

References

1. Caricati-Neto A, Errante PR, Menezes-Rodrigues FS. Emerging a new strategy for the antitumor immunotherapy : pharmacological modulation of the Ca 2 +/Camp signaling interaction. *Arch Microbiol Immunol*. 2017;1(3):89–97. doi:doi:10.26502/ami.93650012
2. Desantis CE, Fedewa SA, Sauer AG, Kramer JL, Smith RA, Jemal A. Breast cancer statistics, 2015 : convergence of incidence rates between black and white women. *A Cancer J Clin*. 2016;66(1):31–42. doi:doi:10.3322/caac.21320.
3. Prados J, Melguizo C, Ortiz R, et al. Doxorubicin-loaded nanoparticles: new advances in breast cancer therapy. *Anticancer Agents Med Chem*. 2012;12(9):1058–1070. doi:doi:10.2174/187152012803529646
4. Huang J, Qian W, Wang L, et al. Functionalized milk-protein-coated magnetic nanoparticles for MRI-monitored targeted therapy of pancreatic cancer. *Int J Nanomedicine*. 2016;11:3087–3099. doi:10.2147/IJN.S92722
5. Meirow D, Nugent D. The effects of radiotherapy and chemotherapy on female reproduction. *Hum Reprod Update*. 2001;7(6):535–543. doi:doi:10.1093/humupd/7.6.535
6. Espinosa A, Di Corato R, Kolosnjaj-Tabi J, Flaud P, Pellegrino T, Wilhelm C. Duality of iron oxide nanoparticles in cancer therapy: amplification of heating efficiency by magnetic hyperthermia and photothermal bimodal treatment. *ACS Nano*. 2016;10(2):2436–2446. doi:10.1021/acsnano.5b07249
7. Foglia S, Ledda M, Fioretti D, et al. In vitro biocompatibility study of sub-5 nm silica-coated magnetic iron oxide fluorescent nanoparticles for potential biomedical application. *Sci Rep*. 2017;7(April):1–13. doi:10.1038/srep46513
8. Wu H, Jin H, Wang C, et al. Synergistic cisplatin/doxorubicin combination chemotherapy for multidrug-resistant cancer via polymeric nanogels targeting delivery. *ACS Appl Mater Interfaces*. 2017;9(11):9426–9436. doi:doi:10.1021/acsami.6b16844
9. Betancourt T, Brown B, Brannon-Peppas L. Doxorubicin-loaded PLGA nanoparticles by nanoprecipitation: preparation, characterization and in vitro evaluation. *Nanomedicine*. 2007;2(2):219–232. doi:doi:10.2217/17435889.2.2.219
10. Liu X, Huang N, Li H, Wang H, Jin Q, Ji J. Multidentate polyethylene glycol modi Fi ed gold nanorods for in vivo near-infrared photothermal cancer therapy. *Appl Mater Interfaces*. 2014;6:5657–5668. doi:doi:10.1021/am5001823
11. Zhang X, Clime L, Roberge H, et al. pH-triggered doxorubicin delivery based on hollow nanoporous silica nanoparticles with free-standing superparamagnetic Fe 3 O 4 cores. *J Phys Chem C*. 2011;115:1436–1443. doi:doi:10.1021/jp1075498
12. Pandey S, Thakur M, Mewada A, Anjarlekar D, Mishra N, Sharon M. Carbon dots functionalized gold nanorod mediated delivery of doxorubicin: tri-functional nano-worms for drug delivery, photothermal therapy and bioimaging. *J Mater Chem B*. 2013;1(38):4972–4982. doi:doi:10.1039/c3tb20761g
13. Khafaji M, Vossoughi M, Hormozi-Nezhad MR, Dinarvand R, Börrnert F, Irajizad A. A new bifunctional hybrid nanostructure as an active platform for photothermal therapy and MR imaging. *Sci Rep*. 2016;6. doi:10.1038/srep27847
14. Elbialy NS, Fathy MM, Reem A-W, et al. Multifunctional magnetic-gold nanoparticles for efficient combined targeted drug delivery and interstitial photothermal therapy. *Int J Pharm*. 2018;554:256–263.
15. Guo D, Ji X, Wang H, et al. Silicon nanowire-based multifunctional platform for chemo-photothermal synergistic cancer therapy. *J Mater Chem B*. 2018;6(23):3876–3883. doi:10.1039/C7TB02907A
16. Sivakumar B, Aswathy RG, Romero-Aburto R, et al. Highly versatile SPION encapsulated PLGA nanoparticles as photothermal ablators of cancer cells and as multimodal imaging agents. *Biomater Sci*. 2017;5(3):432–443. doi:doi:10.1039/c6bm00621c
17. Oh Y, Je JY, Moorthy MS, Seo H, Cho WH. pH and NIR-light-responsive magnetic iron oxide nanoparticles for mitochondria-mediated apoptotic cell death induced by chemo-photothermal therapy. *Int J Pharm*. 2017;531(1):1–13. doi:doi:10.1016/j.ijpharm.2017.07.014
18. Liang P, Chen Y-C, Chiang C, et al. Doxorubicin-modified magnetic nanoparticles as a drug delivery system for magnetic resonance chemotherapy. *Int J Nanomedicine*. 2016;11:2021–2037. doi:doi:10.2147/IJN.S94139
19. Hurley KR, Ring HL, Etheridge M, et al. Predictable heating and positive MRI contrast from a mesoporous silica-coated iron oxide nanoparticle. *Mol Pharm*. 2016;13(7):2172–2183. doi:doi:10.1021/acs.molpharmaceut.5b00866
20. Yang Y, Liu J, Sun X, et al. Near-infrared light-activated cancer cell targeting and drug delivery with aptamer-modified nanostructures. *Nano Res*. 2016;9(1):139–148. doi:doi:10.1007/s12274-015-0898-4
21. Kossatz S, Grandke J, Couleaud P, et al. Efficient treatment of breast cancer xenografts with multifunctionalized iron oxide nanoparticles combining magnetic hyperthermia and anti-cancer drug delivery. *Breast Cancer Res*. 2015;17(1):1–17. doi:10.1186/s13058-015-0576-1
22. Benyettou F, Ocadiz Flores JA, Ravaux F, et al. Mesoporous γ-iron oxide nanoparticles for magnetically triggered release of doxorubicin and hyperthermia treatment. *Chem - A Eur J*. 2016;22(47):17020–17028. doi:10.1002/chem.201602956
23. Hu Y, Hu H, Yan J, et al. Multifunctional porous iron oxide nanoagents for MRI and photothermal/chemo synergistic therapy. *Bioconjug Chem*. 2018;29(4):1283–1290. doi:10.1021/acs.bioconjchem.8b00052
24. Lee S, George Thomas R, Ju Moon M, et al. Near-infrared heptamethine cyanine based iron oxide nanoparticles for tumor targeted multimodal imaging and photothermal therapy. *Sci Rep*. 2017;7(1):1–14. doi:doi:10.1038/s41598-017-01108-5
25. Wu M, Zhang D, Zeng Y, Wu L, Liu X, Liu J. Nanocluster of superparamagnetic iron oxide nanoparticles coated with poly (dopamine) for magnetic field-targeting, highly sensitive MRI and photothermal cancer therapy. *Nanotechnology*. 2015;26(11):115102. doi:doi:10.1088/0957-4484/26/11/115102

26. Luo X, Wang Y, Lin H, Qu FDOX. Fe 3 O 4@ mSiO 2-PO-FA nanocomposite for synergistic chemo-and photothermal therapy. *RSC Adv*. 2016;6(113):112232–112240. doi:10.1039/C6RA23292B
27. Yang Y, Wang C, Tian C, Guo H, Shen Y, Fe ZM. 3 O 4@ MnO 2@ PPy nanocomposites overcome hypoxia: magnetic-targeting-assisted controlled chemotherapy and enhanced photodynamic/photothermal therapy. *J Mater Chem B*. 2018;6(42):6848–6857. doi:10.1039/C8TB02077A
28. Xie W, Gao Q, Wang D, et al. Doxorubicin-loaded Fe 3 O 4@ MoS 2-PEG-2DG nanocubes as a theranostic platform for magnetic resonance imaging-guided chemo-photothermal therapy of breast cancer. *Nano Res*. 2018;11(5):2470–2487. doi:10.1007/s12274-017-1871-1
29. Chen M-L, Gao Z-W, Chen X-M, Pang S-C ZY. Laser-assisted in situ synthesis of graphene-based magnetic-responsive hybrids for multimodal imaging-guided chemo/photothermal synergistic therapy. *Talanta*. 2018;182:433–442. doi:10.1016/j.talanta.2018.02.030
30. Chen H, Liu F, Lei Z, Ma L, Wang Z. Fe 2 O 3@ Au core@ shell nanoparticle–graphene nanocomposites as theranostic agents for bioimaging and chemo-photothermal synergistic therapy. *RSC Adv*. 2015;5(103):84980–84987. doi:10.1039/C5RA17143A
31. Seabra AB, Paula AJ, de Lima R, Alves OL, Duran N. Nanotoxicity of graphene and graphene oxide. *Chem Res Toxicol*. 2014;27(2):159–168. doi:10.1021/tx400385x
32. Li R, Guiney LM, Chang CH, et al. Surface oxidation of graphene oxide determines membrane damage, lipid peroxidation, and cytotoxicity in macrophages in a pulmonary toxicity model. *ACS Nano*. 2018;12(2):1390–1402. doi:10.1021/acsnano.7b07737
33. Lele BS, Kulkarni MG. Single step room temperature oxidation of poly(ethylene glycol) to poly(oxyethylene)-dicarboxylic acid. *J Appl Polym Sci*. 1998;70(5):883–890. doi:10.1002/(ISSN)1097-4628
34. Morel A-L, Nikitenko SI, Gionnet K, et al. Sonochemical approach to the synthesis of Fe3O4@SiO2 core−shell nanoparticles with tunable properties. *ACS Nano*. 2008;2(5):847–856. doi:10.1021/nn800091q
35. Zhu Y, Ikoma T, Hanagata N, Kaskel S. Rattle-type Fe3O4@SiO2 hollow mesoporous spheres as carriers for drug delivery. *Small*. 2010;6(3):471–478. doi:doi:10.1002/smll.200901403
36. Ding HL, Zhang YX, Wang S, Xu JM, Xu SC, Li GH. Fe3O4@SiO2core/shell nanoparticles: the silica coating regulations with a single core for different core sizes and shell thicknesses. *Chem Mater*. 2012;24(23):4572–4580. doi:10.1021/cm302828d
37. Fan H-L, Zhou S-F, Qi G-S, Liu Y-Z. Continuous preparation of Fe3O4 nanoparticles using impinging stream-rotating packed bed reactor and magnetic property thereof. *J Alloys Compd*. 2016;662:497–504. doi:10.1016/j.jallcom.2015.12.025
38. Fidale LC, Nikolajski M, Rudolph T, Dutz S, Schacher FH, Heinze T. Hybrid Fe3O4@ amino cellulose nanoparticles in organic media–heterogeneous ligands for atom transfer radical polymerizations. *J Colloid Interface Sci*. 2013;390(1):25–33. doi:10.1016/j.jcis.2012.09.019
39. Lee J, Isobe T, Senna M. Preparation of ultrafine Fe3O4Particles by precipitation in the presence of PVA at high pH. *J Colloid Interface Sci*. 1996;177(2):490–494. doi:10.1006/jcis.1996.0062
40. Zhang C, Wängler B, Morgenstern B, et al. Silica-and alkoxysilane-coated ultrasmall superparamagnetic iron oxide particles: a promising tool to label cells for magnetic resonance imaging. *Langmuir*. 2007;23(3):1427–1434. doi:10.1021/la061879k
41. Pozzi D, Colapicchioni V, Caracciolo G, et al. Effect of polyethyleneglycol (PEG) chain length on the bio-nano- interactions between PEGylated lipid nanoparticles and biological fluids: from nanostructure to uptake in cancer cells. *Nanoscale*. 2014;6(5):2782–2792. doi:doi:10.1039/c3nr05559k
42. Murugan K, Choonara YE, Kumar P, Bijukumar D, Du Toit LC, Pillay V. Parameters and characteristics governing cellular internalization and trans-barrier trafficking of nanostructures. *Int J Nanomedicine*. 2015;10:2191.
43. Prijic S, Scancar J, Romih R, et al. Increased cellular uptake of biocompatible superparamagnetic iron oxide nanoparticles into malignant cells by an external magnetic field. *J Membr Biol*. 2010;236(1):167–179. doi:doi:10.1007/s00232-010-9271-4
44. Silva AH, Lima E, Mansilla MV, et al. Superparamagnetic iron-oxide nanoparticles mPEG350- and mPEG2000-coated: cell uptake and biocompatibility evaluation. *Nanomed Nanotechnol Biol Med*. 2016;12(4):909–919. doi:doi:10.1016/j.nano.2015.12.371
45. Zhao Y, Sun X, Zhang G, Trewyn BG, Slowing II, Lin VS-Y. Interaction of mesoporous silica nanoparticles with human red blood cell membranes: size and surface effects. *ACS Nano*. 2011;5(2):1366–1375. doi:doi:10.1021/nn103077k
46. Hu Q, Zhang Y, Wang C, et al. Hemocompatibility evaluation in vitro of methoxy polyethyleneglycol-polycaprolactone copolymer solutions. *J Biomed Mater Res - Part A*. 2016;104(3):802–812. doi:doi:10.1002/jbm.a.35594
47. Bender EA, Adorne MD, Colomé LM, Abdalla DSP, Guterres SS, Pohlmann AR. Hemocompatibility of poly(ε-caprolactone) lipid-core nanocapsules stabilized with polysorbate 80-lecithin and uncoated or coated with chitosan. *Int J Pharm*. 2012;426(1):271–279. doi:10.1016/j.ijpharm.2012.01.051
48. Zhang Z, Wang J, Nie X, et al. Near infrared laser-induced targeted cancer therapy using thermoresponsive polymer encapsulated gold nanorods. *J Am Chem Soc*. 2014;136(20):7317–7326. doi:10.1021/ja412735p
49. Kumar CSSR, Mohammad F. Magnetic nanomaterials for hyperthermia-based therapy and controlled drug delivery. *Adv Drug Deliv Rev*. 2011;63(9):789–808. doi:10.1016/j.addr.2011.03.008
50. Ma P, Xiao H, Yu C, et al. Enhanced cisplatin chemotherapy by iron oxide nanocarrier-mediated generation of highly toxic reactive oxygen species. *Nano Lett*. 2017;17(2):928–937. doi:10.1021/acs.nanolett.6b04269
51. Wang X, Teng Z, Wang H, et al. Increasing the cytotoxicity of doxorubicin in breast cancer MCF-7 cells with multidrug resistance using a mesoporous silica nanoparticle drug delivery system. *Int J Clin Exp Pathol*. 2014;7(4):1337–1347.
52. Shrikhande SS, Jain DS, Athawale RB, et al. Evaluation of antimetastatic potential of Cisplatin polymeric nanocarriers on B16F10 melanoma cells. *Saudi Pharm J*. 2015;23(4):341–351. doi:10.1016/j.jsps.2014.08.004
53. Byeon HJ, Thao LQ, Lee S, et al. Doxorubicin-loaded nanoparticles consisted of cationic- and mannose-modified-albumins for dual-targeting in brain tumors. *J Control Release*. 2016;225:301–313. doi:10.1016/j.jconrel.2016.01.046
54. Lau JKC, Deubel DV. Hydrolysis of the anticancer drug cisplatin: pitfalls in the interpretation of quantum chemical calculations. *J Chem Theory Comput*. 2006;2(1):103–106. doi:10.1021/ct050229a
55. Štarha P, Smola D, Tuček J, Trávníček Z. Efficient synthesis of a maghemite/gold hybrid nanoparticle system as a magnetic carrier for the transport of platinum-based metallotherapeutics. *Int J Mol Sci*. 2015;16(1):2034–2051. doi:10.3390/ijms16012034
56. Thapa B, Diaz-Diestra D, Beltran-Huarac J, Weiner BR, Morell G. Enhanced MRI T2Relaxivity in contrast-probed anchor-free PEGylated iron oxide nanoparticles. *Nanoscale Res Lett*. 2017;12:1–13. doi:10.1186/s11671-017-2084-y
57. Bian X, Song ZL, Qian Y, et al. Fabrication of graphene-isolated-au-nanocrystal nanostructures for multimodal cell imaging and photothermal-enhanced chemotherapy. *Sci Rep*. 2014;4:29–32. doi:10.1038/srep06093
58. Li L, Nurunnabi M, Nafiujjaman M, Jeong YY, Lee YK, Huh KM. A photosensitizer-conjugated magnetic iron oxide/gold hybrid nanoparticle as an activatable platform for photodynamic cancer therapy. *J Mater Chem B*. 2014;2(19):2929–2937. doi:10.1039/c4tb00181h
59. Lin Y, Wang S, Zhang Y, et al. Ultra-high relaxivity iron oxide nanoparticles confined in polymer nanospheres for tumor MR imaging. *J Mater Chem B*. 2015;3(28):5702–5710. doi:10.1039/c5tb00593k
60. Di H, Wu H, Gao Y, Li W, Zou D, Dong C. Doxorubicin- and cisplatin-loaded nanostructured lipid carriers for breast cancer combination chemotherapy. *Drug Dev Ind Pharm*. 2016;42(12):2038–2043. doi:10.1080/03639045.2016.1190743

61. Tahover E, Patil YP, Gabizon AA. Emerging delivery systems to reduce doxorubicin cardiotoxicity and improve therapeutic index: focus on liposomes. *Anticancer Drugs*. 2015;26(3):241–258. doi:10.1097/CAD.0000000000000182
62. Ma P, Xiao H, Li C, et al. Inorganic nanocarriers for platinum drug delivery. *Mater Today*. 2015;18(10):554–564. doi:10.1016/j.mattod.2015.05.017
63. Hu Q, Sun W, Wang C, Gu Z. Recent advances of cocktail chemotherapy by combination drug delivery systems. *Adv Drug Deliv Rev*. 2016;98:19–34. doi:10.1016/j.addr.2015.10.022
64. Unsoy G, Khodadust R, Yalcin S, Mutlu P, Gunduz U. Synthesis of Doxorubicin loaded magnetic chitosan nanoparticles for pH responsive targeted drug delivery. *Eur J Pharm Sci*. 2014;62:243–250. doi:10.1016/j.ejps.2014.05.021
65. Wang F, Wang Y-C, Dou S, Xiong M-H, Sun T-M, Wang J. Doxorubicin-tethered responsive gold nanoparticles facilitate intracellular drug delivery for overcoming multidrug resistance in cancer cells. *ACS Nano*. 2011;5(5):3679–3692. doi:10.1021/nn200007z
66. Swietach P, Vaughan-Jones RD, Harris AL, Hulikova A. The chemistry, physiology and pathology of pH in cancer. Philos Trans R Soc B. 2014.
67. Alkilany AM, Nagaria PK, Hexel CR, Shaw TJ, Murphy CJ, Wyatt MD. Cellular uptake and cytotoxicity of gold nanorods: molecular origin of cytotoxicity and surface effects. *Small*. 2009;5(6):701–708. doi:10.1002/smll.200801546
68. Quinto CA, Mohindra P, Tong S, Bao G. Multifunctional superparamagnetic iron oxide nanoparticles for combined chemotherapy and hyperthermia cancer treatment. *Nanoscale*. 2015;7(29):12728–12736. doi:10.1039/c5nr02718g
69. Ehlerding EB, Chen F, Biodegradable CW. Renal Clearable Inorganic Nanoparticles. *Adv Sci*. 2016;3(2):1500223. doi:10.1002/advs.201500223
70. Kievit FM, Zhang M. Surface engineering of iron oxide nanoparticles for targeted cancer therapy. *Acc Chem Res*. 2011;44(10):853–862. doi:10.1021/ar2000277
71. Kapse-Mistry S, Govender T, Srivastava R, Yergeri M. Nanodrug delivery in reversing multidrug resistance in cancer cells. *Front Pharmacol*. 2014;5:159.
72. Wang X, Zhang R, Wu C, et al. The application of Fe3O4 nanoparticles in cancer research: a new strategy to inhibit drug resistance. *J Biomed Mater Res Part A*. 2007;80A(4):852–860. doi:10.1002/jbm.a.30901
73. Chen Y, Zhang F, Wang Q, et al. The synthesis of LA-Fe 3 O 4@ PDA-PEG-DOX for photothermal therapy–chemotherapy. *Dalt Trans*. 2018;47(7):2435–2443. doi:10.1039/C7DT04080F
74. Liu B, Zhang X, Li C, et al. Magnetically targeted delivery of DOX loaded Cu 9 S 5@ mSiO 2@ Fe 3 O 4-PEG nanocomposites for combined MR imaging and chemo/photothermal synergistic therapy. *Nanoscale*. 2016;8(25):12560–12569. doi:10.1039/C5NR06322A